

submitted to ApJ

A Radio Nebula Surrounding the Ultraluminous X-Ray Source in NGC 5408

Cornelia C. Lang, Philip Kaaret

Department of Physics and Astronomy

University of Iowa, Van Allen Hall, Iowa City, IA 52242, USA

`cornelia-lang@uiowa.edu`

Stéphane Corbel

AIM–Unité Mixte de Recherche CEA–CNRS

*Université Paris VII–UMR 7158, CEA Saclay, Service d’Astrophysique, F–491191 Gif sur
Yvette, France.*

and

Allison Mercer

Department of Physics and Astronomy

University of Iowa, Van Allen Hall, Iowa City, IA 52242, USA

ABSTRACT

New radio observations of the counterpart of the ultraluminous X-ray source in NGC 5408 show for the first time that the radio emission is resolved with an angular size of $1.5''$ to $2.0''$. This corresponds to a physical size of 35–46 pc, and rules out interpretation of the radio emission as beamed emission from a relativistic jet. In addition, the radio spectral index of the counterpart is well determined from three frequencies and found to be $\alpha = -0.8 \pm 0.2$. The radio emission is likely to be optically-thin synchrotron emission from a nebula surrounding the X-ray source. The radio luminosity of the counterpart is 3.8×10^{34} erg s $^{-1}$ and the minimum energy required to power the nebula is $\sim 1 \times 10^{49}$ erg. These values are two orders of magnitude larger than in any Galactic nebula powered by an accreting compact object.

Subject headings: black hole physics – galaxies: individual: NGC 5408 galaxies: stellar content – X-rays: galaxies – X-rays: black holes

1. Introduction

Ultraluminous x-ray sources (ULXs) are non-nuclear x-ray sources in external galaxies with apparent luminosities above the Eddington limit for a $20M_{\odot}$ black hole, the maximum mass of any dynamically-measured black hole mass in the Galaxy (Remillard & McClintock 2006); for a review, see Fabbiano (2006). ULXs with strong variability are likely accreting objects and may either be “intermediate mass” black holes (Colbert & Mushotzky 1999; Makishima et al. 2000; Kaaret et al. 2001) or normal (stellar-mass) black holes with beamed or super Eddington radiation (King et al. 2001; Körding et al. 2002; Begelman 2002). The ULX in the dwarf irregular galaxy NGC 5408 (NGC 5408 X-1) is variable and is one of the few ULXs with a known radio counterpart (Kaaret et al. 2003). The radio emission could arise directly from a relativistic jet beamed toward our line of sight, in which case a stellar-mass black hole would suffice to produce the radio and X-ray emission, or from a nebula surrounding the compact object. Recent radio observations presented by Soria et al. (2006) suggest that the source has a steep spectrum ($\alpha < -1$), but show no indication of radio flux density variability.

In order to better understand the nature of the radio emission from NGC 5408 X-1, we obtained new joint observations in the radio using the Very Large Array (VLA) of the National Radio Astronomy Observatory¹ and in the X-ray using the *Chandra X-Ray Observatory*. In addition, because the target is a low-declination source ($\delta \sim -41^{\circ}$), we present new and archival radio observations from the Australia Telescope Compact Array (ATCA). Finally, we also reanalyzed archival optical observations made using the *Hubble Space Telescope* (HST). We describe the observations and data reduction in § 2, present our results in § 3, and discuss the interpretation in § 4.

2. Observations and Analysis

2.1. VLA Observations

VLA observations of the ULX source in NGC 5408 were made at 4.9 GHz (6 cm) with four different array configurations between December 2003 and January 2005 : A, BnA, B, and CnB (see Table 1). Each observation was approximately 3.5 hours long and corresponds to a joint *Chandra* X-ray observation. Standard procedures were carried out for flux and phase calibration using the Astronomical Imaging Processing System (AIPS) of the NRAO.

¹The National Radio Astronomy Observatory is a facility of the National Science Foundation operated under cooperative agreement by Associated Universities, Inc.

We used the flux density calibrator, J1331+305, and the phase calibrator, J1353-441, a source which is located within 3° of the target. For all observations, fast switching between the target source and calibrator was used with a cycle time for the calibrator-source pair of 2.5 to 3 minutes (with 45 seconds on the calibrator and 90 to 120 seconds on the source).

The VLA image resolutions vary between $1.01'' \times 0.28''$ (A-array) and $6.01'' \times 3.30''$ (CnB-array). Because of the proximity of the bright starburst region in NGC5408 and the weak radio emission associated with the ULX, obtaining an accurate flux density for this source is difficult. However, with the high resolution of the VLA A, BnA and B-arrays, it is possible to distinguish the radio emission associated with the ULX from the extended emission from the starburst region in most of our images.

In fact, in attempting to determine the accurate flux density and source structure, the extended emission from this starburst region turns out to be a key issue. One way to examine the contribution of the extended emission is to adjust the imaging weighting function. The Briggs’ ROBUST parameter controls the data weights in the (u,v) plane. Positive values of the ROBUST parameter (1 to 5) bring out the more extended structure by weighting the inner part of the (u,v) plane more heavily (“natural weighting”). Such values will increase the signal to noise on extended features but lower the spatial resolution. Negative values of the ROBUST parameter (-1 to -5) give more equal weight to all points in the (u,v) plane (“uniform weighting”) which tends to maximize spatial resolution but at the cost of signal to noise. A ROBUST=0 is balanced between these extremes. As many four images were made from data for an individual array using varying ROBUST parameters.

In addition, a more quantitative way to remove extended flux is to limit the range of (u,v) baselines used for imaging. In cases where the emission from the ULX is contaminated by extended flux from the starburst, a (u,v) cutoff of $5 \text{ k}\lambda$ was applied. This cutoff limits flux on angular size scales larger than $\sim 6''$. For the VLA-B and VLA-CnB array images, where extended flux is present, such cutoffs have been applied.

2.2. ATCA Observations

We also made continuum radio observations of NGC 5408 using the Australia Telescope Compact Array (ATCA) located in Narrabri, New South Wales, Australia. The ATCA consists of five 22-m antennas positioned along an E-W track with a short N-S spur and a sixth antenna at a fixed location. We obtained three new ATCA observations of 12 hours each on consecutive days with the 6 km configuration 6.0A (6A). This provides the best angular resolution possible with ATCA ($\sim 1''$ at 4.8 GHz). For the first two observations,

we switched the feed-horns at roughly one hour intervals observing in either the 6 cm band (4.8 GHz) or the 13 and 20 cm bands (1.4 and 2.4 GHz). The duty cycle of the switching was arranged so the integration at 6 cm was four times as long as those at 13 and 20 cm. On the last day, we observed with the 5 cm band (6.1 GHz) instead of the 6 cm band (4.8 GHz).

J1934-638 and J1349-439 were used for flux and phase calibration. Editing, calibration, imaging and analysis were performed using standard routines in the MIRIAD software package (Sault & Killeen 1998). A radio counterpart to the ULX was detected at all frequencies. Because of the low declination of NGC 5408, the ATCA forms a more symmetric synthesized beam than the VLA. The extended emission associated with the starburst in NGC 5408 is present, but in the ATCA images, the radio counterpart to the ULX is clearly distinguished, especially in the 6A configuration data at 4.8, 6.2 GHz. However, at the lower frequencies (1.4 and 2.3 GHz) there is still contamination from the starburst. During imaging, a variety of ROBUST parameters were also used to downweight the extended emission, similar to the procedure in the VLA imaging. In addition, we analyzed archival ATCA observations of NGC 5408 at a range of frequencies, observed during 2000-2004 (listed in Table 2). In the several of the ATCA datasets, (e.g., the 6D-array 4.9 GHz data (Kaaret et al. (2003), and the 2.3 and 1.4 GHz archival datasets) a (u,v) cutoff range of $3 \text{ k}\lambda$ was used to remove flux on extended scales larger than $11''$.

2.3. X-ray Observations

NGC 5408 was observed with the *Chandra X-Ray Observatory* (Weisskopf 1988) five times using the ACIS spectroscopic array (ACIS-S; Bautz et al. 1998) in imaging mode and the High-Resolution Mirror Assembly (HRMA; van Speybroeck et al. 1997). The observations began in 2002 and ended in 2005, see Table 1. Because a high X-ray count rate was expected, only the S3 chip was operated with a 1/4 sub-array mode for the first observation and a 1/8 sub-array for the other observations. This gave an exposure time of 0.8 s for the first observation and 0.4 s for the others. For each observation, we constructed an image using all valid events on the S3 chip and used the *wavdetect* tool which is part of the *CIAO* data analysis package to search for X-ray sources. Typically only the ULX was detected in each observation. The position of the ULX was within $0.23''$ of $\text{RA} = 14\text{h}03\text{m}19.63\text{s} \pm 0.01\text{s}$, $\text{DEC} -41\text{d}22'58.65'' \pm 0.2''$ (J2000) in all observations.

We fit the X-ray spectrum of the ULX for each observation using the *XSPEC* spectral fitting tool which is part of the *LHEASOFT* X-ray data analysis package and response matrices calculated using *CIAO*. As previously reported by Kaaret et al. (2003), we found

that absorbed single power-law models did not provide an adequate fits (except for the last observation), while models consisting of either an absorbed broken power-law or the absorbed sum of a multicolor disk blackbody plus a power-law did provide adequate fits. There were no pronounced changes in spectra shape between the different observations. The fit parameters were similar to those quoted in Kaaret et al. (2003). The flux for each observation calculated using the fitted multicolor disk blackbody plus power-law model are given in Table 1. We also did not observe any significant changes in the X-ray flux level between observations.

2.4. HST Observations

Two WFPC2 observations of NGC 5408 are present in the *Hubble Space Telescope* (HST) archive. The observations were obtained as part of a snapshot survey of nearby dwarf galaxy candidates (GO-8601, PI Seitzer) and consist of 600 s WFPC2 exposures with the F606W and F814W filters obtained on 4 July 2000. After extracting the data from the HST archive, we used IRAF to mosaic and clean the images. We corrected the absolute astrometry of the HST image using stars from the 2MASS catalog (Skrutskie et al. 2006) using the Graphical Astronomy and Image Analysis Tool (GAIA). We used only 2MASS sources on the WF3 chips where the ULX is located in order to preclude issues regarding the relative positioning of the WFPC2 chips. We estimate that the astrometric uncertainty is $0.2''$. We used the HSTphot stellar photometry package to obtain photometry (Dolphin 2000). We removed bad pixels, cosmic rays, and hot pixels and then obtained simultaneous photometry for the F606W and F814W images.

3. Results

3.1. Radio Counterpart

The flux density of the radio emission associated with the ULX in the VLA and ATCA images was measured by fitting a 2-D Gaussian point source to the peak radio emission in each of the various images. In all cases, the source appears to be point-like with slightly extended emission, but nothing which we can confidently resolve. The radio source position from our VLA B-array image (resolution of $3.17'' \times 0.92''$) is RA, DEC (J2000) = $14\text{h}03\text{m}19.63\text{s} \pm 0.01\text{s}$, $-41\text{d}22' 58.7'' \pm 0.2''$, which is within $0.1''$ of the ULX position calculated from the *Chandra* observations (Kaaret et al. 2003). This is well within the *Chandra* error circle. Using the ATCA 4.8 GHz and 6.1 GHz data, the position of the radio source is RA, DEC (J2000) = $14\text{h}03\text{m}19.61\text{s} \pm 0.02\text{s}$, $-41\text{d}22'58.5'' \pm 0.2''$.

3.1.1. 4.9 GHz Emission

Table 3 lists the measured 4.9 GHz flux density and corresponding ROBUST weighting, array configuration, geometrical beam size ($\sqrt{\theta_{maj}\theta_{min}}$) and an indication of any (u,v) cutoff used in the imaging. Radio emission was detected above 3σ in 20 of the 21 images made at 4.9 GHz from the VLA and ATCA data. The source was not detected in the highest resolution 4.9 GHz VLA image ($1.01'' \times 0.28''$; A-array, Robust=-1) with an upper limit of 0.1 mJy. The largest angular size detectable with the VLA in its A-array configuration is $10''$. The radio source is detected in the other two VLA A-array images, but with modest detections ($\sim 7\sigma$ in both cases). Figure 1 shows the BnA-array image of NGC5408 (Robust=1). The resolution of this image is $1.94'' \times 1.20''$ and the source is clearly detected at the 10σ level.

Figure 2 shows the highest resolution 4.9 GHz ATCA image, which has a beamsize very similar to the VLA BnA-array image shown in Figure 1. In the majority of the VLA and ATCA images, the radio emission associated with NGC 5408 X-1 is obvious and clearly separated from the extended emission associated with the NGC 5408 starburst. However, in cases such as the VLA B-array naturally-weighted image, where the resolution is lower and favors the extended structures, a significant amount of extended emission is present (see Fig. 3, left). Removing the shortest (u,v) baselines ($< 5 \text{ k}\lambda$) for these lower-resolution images produces an image, shown in Fig. 3, right, where the the radio emission associated with NGC 5408 X-1 is clearly separated from the extended emission associated with the starburst.

Figure 4 shows the flux density and associated errors versus the geometric beamsize for measurements from 16 images of VLA (diamonds) and ATCA (square; new and archival) data taken from Table 3. The filled symbols indicate that a (u,v) cutoff was applied to the data in order to remove extended emission which may contaminate the flux density. However, not all measurements were included in Figure 4. Images made with the VLA CnB-array at all robust weightings and with the ATCA 6D configuration have low enough resolution that it is difficult to separate the background emission from NGC 5408 from the radio emission at the position of the ULX. In fact, the flux densities for the VLA CnB-array and ATCA 6D-array measurements are in the range of 0.32 to 0.51 mJy, up to twice as high as measurements made with more extended arrays, indicating that the background contributes significantly to the measurement. For this reason, only the measurements from images where we were confident we were separating out the radio emission associated with NGC 5408 X-1 were used to make Figure 4.

3.1.2. Source Size and Structure

Previously, Soria et al. (2006) had made some of the highest resolution observations of the ULX in NGC 5408 using the ATCA. They measured the flux density in images with beamsizes of $1.5''$ to $3.5''$ and found an essentially flat distribution of flux density with beamsize. However, their observations do not resolve the source and therefore are only consistent with emission from a point source (Soria et al. 2006). The VLA data presented here for the first time probe even higher angular resolutions ($0.5''$ to $1.5''$). Figure 4 shows that the VLA data are crucial in studying the flux density versus geometric beam size for scales $< 1.5''$. There is a clear trend of decreasing flux density at smaller beamsizes below a geometric beamsize of $1.5''$. The linear rise of flux density with beamsize shown in Figure 4 indicates that there is extended emission associated with this source on beamsize scales between $\sim 0.5''$ and $\sim 1.5''$. For beamsizes greater than $\sim 1.5''$, the flux density measurements are relatively constant (within the errors), suggesting the source has an angular extent in the range of $1.5''$ to $2.0''$.

3.1.3. Variability

Because the radio source associated with the ULX is likely to be somewhat extended, different configurations of the VLA radio telescope will be sensitive to emission on differing angular size scales. Therefore, it is not possible to look for flux variability in our high-resolution VLA observations (where the configuration ranges from A-array to CnB-array). However, ATCA observations over a number of epochs (e.g., Kaaret et al. (2003), Soria et al. (2006), and this paper) have shown that the flux density at 4.9 GHz does not appear to vary significantly and has an average, overall value near 0.20 mJy.

3.1.4. Multifrequency Data and Spectral Index

Multi-frequency observations at 1.4, 2.3, 4.9 and 6.1 GHz were made as part of the new ATCA data presented here. At each frequency, all existing ATCA data were combined (see Table 2) and a point source was fit to the radio emission associated with the ULX. We find flux densities of 0.62 ± 0.10 mJy at 1.4 GHz (geometric beam size of $6.7''$; ROBUST= -5 ; (u,v) cutoff < 5 k λ), 0.37 ± 0.08 mJy at 2.4 GHz (geometric beam size of $3.3''$; ROBUST= -5), 0.20 ± 0.03 mJy at 4.9 GHz (geometric beam size= $1.5''$, ROBUST= -5) and 0.17 ± 0.03 at 6.1 GHz. At 1.4 GHz, the contribution from the extended background may be present even though we used uniform weighting and limited the shortest (u,v) data; the beamsize is

large. At 2.3 GHz, the image is made with uniform weighting and the contribution from the extended starburst region is not apparent. Therefore, we determine the spectral index based on the 2.4, 4.9 and 6.1 GHz measurements only and obtain $\alpha = -0.8 \pm 0.2$, where $S_\nu \propto \nu^\alpha$. Figure 5 shows the flux density versus frequency and includes the 1.4 GHz measurement as well as the 8.5 GHz ATCA upper limit from Kaaret et al. (2003). Although not included in the fit, the 1.4 and 8.5 GHz measurements are consistent with the fitted spectral index.

3.2. Optical counterpart

Figure 6 shows the HST/WFPC2 image in the F606W filter for the area near the ULX. The circle drawn on the figure is centered at the VLA source position quoted above and has a radius of $0.28''$, which represents the relative position uncertainty including both the radio position uncertainty and the optical astrometry uncertainty. Only one object lies within the error circle. It is located at a position of RA, DEC (J2000) = 14h03m19.62s, $-41^{\circ}22'58.54''$ (J2000) which is $0.17''$ from the radio position and well inside the error circle. The next closest HST source is $0.43''$ from the VLA position and is outside the error circle. We identify the HST source within the error circle as the likely optical counterpart of the ULX.

The optical counterpart has magnitudes, in the WFPC2 flight photometric system, of 22.387 ± 0.021 in the F606W filter and 22.396 ± 0.043 in the F814W filter (Dolphin 2000). The equivalent Johnson-Cousins magnitudes are $V = 22.4$ and $I = 22.4$. We corrected for reddening using an extinction $E(B - V) = 0.068$ based on the dust maps of Schlegel, Finkbeiner, & Davis (1998) and using an $R_V = 3.1$ extinction curve. The dereddened magnitudes are $V_0 = 22.2$ and $I_0 = 22.3$ and the color is $V_0 - I_0 = -0.1 \pm 0.1$.

4. Discussion

The radio counterpart size of $1.5''$ to $2.0''$ corresponds to a physical diameter of 35–46 pc at the distance of 4.8 Mpc to NGC 5408, as determined by from the tip of the red giant branch Karachentsev et al. (2002). Therefore, we can rule out the interpretation of the radio emission associated with the NGC 5408 ULX as a relativistically beamed jet (Kaaret et al. 2003).

The radio surface brightness of NGC 5408 at 4.9 GHz is $\sim 4 \times 10^{-20} \text{ W m}^{-2} \text{ Hz}^{-1} \text{ sterad}^{-1}$, assuming a source size of $1.5''$. Taking a spectral index of -0.8 , we can calculate the surface brightness at 1.4 GHz in order to compare to values for known supernova remnants of similar sizes (Green 2004). The value of $\sim 1 \times 10^{-19} \text{ W m}^{-2} \text{ Hz}^{-1} \text{ sterad}^{-1}$ is significantly

higher than that of known supernova remnants of similar size. It is therefore more likely that the radio emission associated with NGC 5408 X-1 arises instead from an extended radio lobe. The radio spectrum ($\alpha=-0.8$) of this source is consistent with optically-thin synchrotron emission.

For comparison, the radio nebula W50 surrounds the relativistic jet source SS 433 (Margon 1984) and is thought to be powered by the relativistic outflow. SS 433 has been suggested as a possible Galactic analog to the ULXs (Fabrika & Mescheryakov 2001; Begelman 2006). The radio nebula in W50 is interesting because the nebular radio emission is unlikely to be beamed. The physical size of W50 is roughly 50 pc and is similar to what we estimate for the radio nebula surrounding NGC 5408 X-1. The radio spectral indexes of the various components of W50 range from -0.5 to -0.8 , also consistent with the spectral index of the radio emission in NGC 5408 X-1 ($\alpha \sim -0.8$). A comparison of the radio brightness can be made for the two sources. W50 has an integrated flux density at 1.4 GHz of ~ 70 Jy and a distance of ~ 5 kpc (Dubner et al. 1998). Assuming a spectral index of -0.5 , that translates to a 4.9 GHz flux density of 40 Jy, and if it were at the distance of NGC 5408 (4.8 Mpc), its flux density would be $\sim 40 \mu\text{Jy}$. The integrated flux density of NGC 5408 X-1 at 4.9 GHz is $\sim 200 \mu\text{Jy}$, so its radio brightness is more than a factor of 5 greater than that of W50.

We investigate the energetics of the radio lobe assuming radiation via synchrotron emission, equipartition between particles and fields, and equal energy in electrons and baryons. We use a spectral index $\alpha = -0.8$ (see §3.1.4), a lower frequency cutoff of 1.3 GHz, and an upper frequency cutoff of 6.2 GHz. The total radio luminosity of the source is $3.8 \times 10^{34} \text{ erg s}^{-1}$. For a source diameter of 46 pc and a filling factor of unity, we find that the total energy required is $3.6 \times 10^{49} \text{ erg}$, the magnetic field is $16 \mu\text{G}$, and the synchrotron lifetime is ~ 20 Myr. For contrast, for a diameter of 35 pc and a filling factor of 0.1, the total energy required is $9 \times 10^{48} \text{ erg}$, the magnetic field is $39 \mu\text{G}$, and the lifetime is ~ 5 Myr. We note that the estimates of Soria et al. (2006) for the energy content of a synchrotron nebula surrounding NGC 5408 X-1 are about an order of magnitude larger. This is primarily because they assume an electron energy distribution that extends down to a Lorentz factor of 1, while we, conservatively, assume that the electron energy distribution extends only over the range needed to produce the observed radio emission (1.3 to 6.2 GHz).

The total energy content in relativistic electrons in W50 is in the range $(0.5-7) \times 10^{46} \text{ erg}$ (Dubner et al. 1998). The total energy content in relativistic electrons in the radio nebula surrounding NGC 5408 X-1 is at least two orders of magnitude larger. Therefore, if two nebula are similar, then the jet powering the nebula surrounding NGC 5408 X-1 must be at least two orders of magnitude more powerful than that from SS 433 powering W50. The radio lobes powered by the persistent accreting stellar-mass black hole GRS 1758-258

have a radio luminosity of $3 \times 10^{30} \text{ erg s}^{-1}$ and require an energy content of $2 \times 10^{45} \text{ erg}$ (Rodríguez, Mirabel, Martí 1992) and are even less powerful than W50. We note that the ULX Holmberg II X-1 has an associated radio nebula with a total energy similar to that of the NGC 5408 X-1 nebula (Miller et al. 2005).

At the distance to NGC 5408, the absolute magnitude of the optical counterpart would be $M_V = -6.2$. If the light arises only from the stellar companion, then the magnitude and color exclude main sequence and giant stars and require a supergiant star. The absolute magnitude and color are consistent with classification as a B or early A supergiant. The luminosity of such a star would be in the range of $1-5 \times 10^{38} \text{ erg s}^{-1}$. However, the stellar classification is suspect since light may arise from reprocessing of X-rays from the compact object and since the X-ray luminosity ($\sim 10^{40} \text{ erg s}^{-1}$ if the emission is isotropic) exceeds the expected stellar luminosity by a factor of at least 20 and may strongly affect the physical state of the star.

The X-ray to optical flux ratio, defined following van Paradijs & McClintock (1995) as $\xi = B_0 + 2.5 \log F_X$ where F_X is the X-ray flux density at 2 keV in μJy and we approximate $B_0 = V_0$ due to lack of a B-band image, is $\xi = 20.0$. If we use the flux density at 1 keV, this rises to $\xi = 21.1$. These values are higher than those of any high-mass X-ray binary (HMXB), other than LMC X-3, and are in the range typically found for low-mass X-ray binaries (LMXBs). Thus, it is possible that the companion star contributes little to the observed optical emission, e.g., it is not supergiant, and that most of the optical light arises from reprocessing of X-rays, as occurs in LMXBs (Kaaret et al. 2005).

Acknowledgments

PK acknowledges partial support from *Chandra* grant CXC GO4-5035A and a Faculty Scholar Award from the University of Iowa. STSDAS and PyRAF are products of the Space Telescope Science Institute, which is operated by AURA for NASA. The authors also thank Michael Rupen for planning and carrying out the VLA observations.

REFERENCES

- Arnaud, K. A. 1996, *Astronomical Data Analysis Software and Systems V*, 101, 17
- Begelman, M.C. 2002, *ApJ*, 568, L97
- Begelman, M.C., King, A.R., Pringle, J. E. 2006, *MNRAS*, 370, 399

- Bautz, M. W., et al. 1998, Proc. SPIE, 3444, 210
- Colbert, E.J.M. & Mushotzky, R.F. 1999, ApJ, 519, 89
- Dubner, G.M., Holdaway, M., Goss, W.M., Mirabel, I.F. 1998, AJ, 116, 1842
- Dolphin, A.E. 2000, PASP, 112, 1383
- Fabbiano, G. 2006, ARA&A, 44, 323
- Fabrika, S. & Mescheryakov, A. 2001, IAUS, 205, 268
- Green, D.A. 2004, Bull. Astron. Soc. India, 32, 335
- Kaaret, P. et al. 2001, MNRAS, 321, L29
- Kaaret, P., Corbel, S., Prestwich, A.H., Zezas, A. 2003, Science, 299, 365.
- Kaaret, P. 2005, ApJ, 629, 233
- Karachentsev, I.D. et al. 2002, A&A, 385, 21
- King, A.R. et al. 2001, ApJ, 552, L109
- Körding, E. Falcke, H., & Markoff, S. 2002, A&A, 382, L13
- Makishima, K. et al. 2000, ApJ, 535, 632
- Margon, B. 1984, ARA&A, 22, 507
- Miller, N.A, Mushotzky, R.F., Neff, S.G. 2005, ApJ, 623, L109
- Remillard, R. A., & McClintock, J. E. 2006, ARA&A, 44, 49
- Rodríguez, L.F., Mirabel, I.F., Martí, J. 1992, ApJ, 401, L15
- Sault R.J. & Killeen N.E.B. 1998, The Miriad User's Guide, Sydney: Australia Telescope National Facility
- Schlegel, D., Finkbeiner, D., & Davis, M. 1998, ApJ, 500, 525
- Soria, R., Fender, R.P., Hannikainen, D.C., Read, A.M., & Stevens, I.R. 2006, MNRAS, 368, 1527
- Skrutskie, R.M. et al. 2006, AJ, 131, 1163.

van Paradijs, J. & McClintock J.E. in X-Ray Binaries, eds. W.H.G. Lewin, J. van Paradijs, & E.P.J. van den Heuvel, (Cambridge Univ. Press, 1995), pp. 58-125.

van Speybroeck, L. P., Jerius, D., Edgar, R. J., Gaetz, T. J., Zhao, P., & Reid, P. B. 1997, Proc. SPIE, 3113, 89

Weisskopf, M. C. 1988, Space Science Reviews, 47, 47

Table 1. Chandra and VLA Observations of NGC 5408

Date/Time	X-Ray Flux	VLA array
2002-05-07 13:45:47	1.42	–
2003-12-20 13:06:33	1.49	B
2004-02-09 10:29:47	1.58	CnB
2004-12-20 13:14:36	1.47	A
2005-01-29 11:02:49	1.50	BnA

Note. — The table lists the Chandra/VLA observations of NGC 5408 and includes the date and UT time of the start of the Chandra observation (the VLA observations were roughly simultaneous), the ULX X-ray flux in the 0.3-8 keV band in units of 10^{-12} erg cm $^{-2}$ s $^{-1}$ during the observation, and the VLA array configuration.

Table 2. ATCA Observations of NGC 5408

Date/Time	Array	Frequency (GHz)	Reference
2000-04-01 02:09	6D	4.8, 8.6	Kaaret et. al (2003)
2003-03-03 05:31	6A	4.8, 8.6	Archival 1
2003-05-20 22:05	1.5C	1.4	Archival 2
2003-07-27 17:45	6D	1.4	Archival 3
2003-12-07 10:05	6A	2.3, 4.8	this paper
2003-12-08 11:30	6A	2.3, 4.8	this paper
2003-12-09 11:02	6A	2.3, 6.1	this paper
2004-12-09 to 12-11	6D	1.4, 2.3	Soria et al. (2006)
2004-12-09 to 12-11	6D	4.8, 6.1	Soria et al. (2006)

Note. — The table lists the ATCA observations of NGC 5408 and includes the observation date, the frequency or frequencies of observation, and the measured flux density.

Table 3. 4.9 GHz Flux Density of NGC 5408

Telescope Array	Robust Weight	Flux Density (mJy)	Geometric Beamsize	(u,v) cutoff
VLA-A	-1	$<0.10\pm0.03$	0.53	
VLA-A	1	0.13 ± 0.02	0.75	
VLA-A	3	0.14 ± 0.02	0.83	
VLA-BnA	-1	0.15 ± 0.03	1.17	
VLA-BnA	1	0.20 ± 0.02	1.53	
VLA-BnA	3	0.23 ± 0.02	1.70	
VLA-B	-1	0.21 ± 0.03	1.71	
VLA-B	0	0.23 ± 0.03	1.93	
VLA-B	-5	0.20 ± 0.03	1.62	
VLA-B	5	0.23 ± 0.02	2.66	$< 5 \text{ k}\lambda$
ATCA-6A	-5	0.21 ± 0.03	1.57	
ATCA-6A	0	0.20 ± 0.03	1.89	
ATCA-6A	2	0.19 ± 0.02	3.25	
ATCA-6A	5	0.19 ± 0.02	3.24	
ATCA-6D	-5	0.25 ± 0.06	1.59	$< 3 \text{ k}\lambda$
ATCA-6D	5	0.18 ± 0.04	3.18	$< 3 \text{ k}\lambda$
VLA-CnB	0	0.51 ± 0.03	4.45	
VLA-CnB	-5	0.46 ± 0.04	3.77	
VLA-CnB	-5	0.32 ± 0.04	3.71	$< 5 \text{ k}\lambda$
VLA-CnB	-1	0.47 ± 0.03	4.08	
ATCA-6D	5	0.43 ± 0.04	3.46	

Note. — The table lists the 4.9 GHz flux densities for the radio counterpart of the ULX in NGC5408. All fits are for an unresolved point source. It is not possible to distinguish between the source and background emission for the measurements listed below the horizontal line.

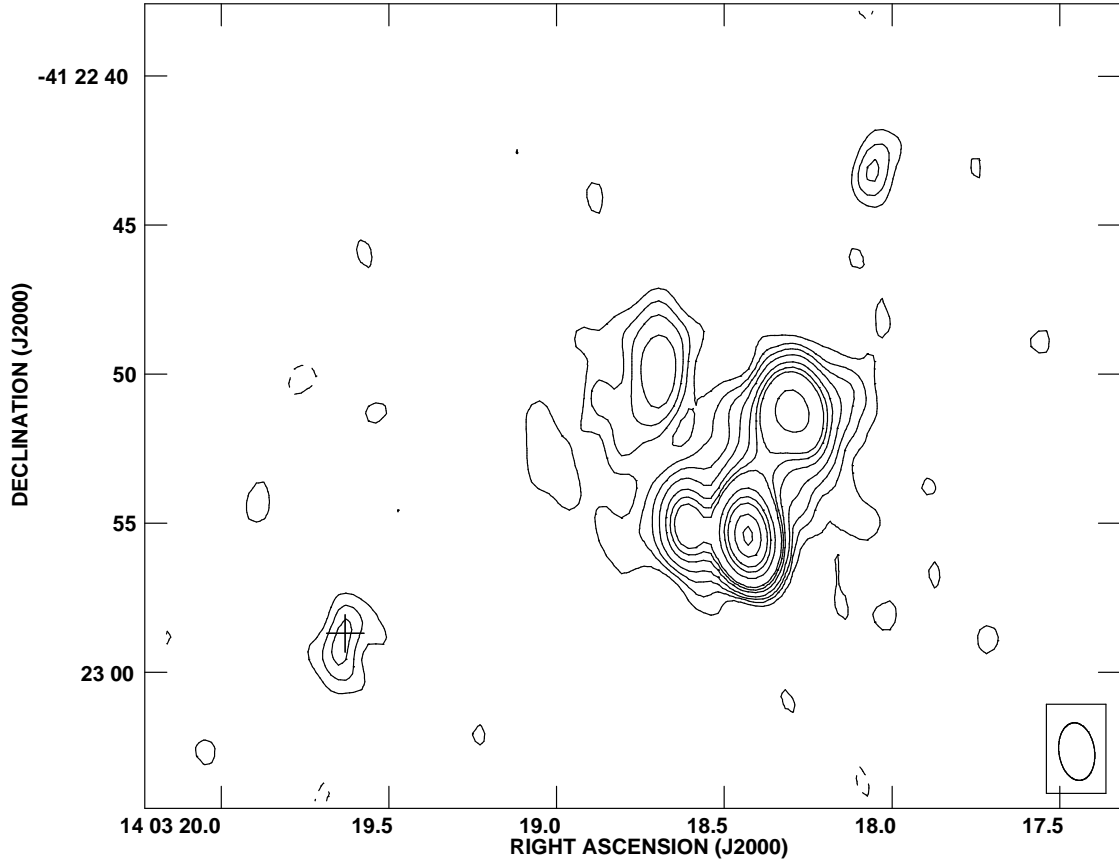


Fig. 1.— VLA 4.9 GHz BnA-array image of the radio emission in NGC5408. The compact radio source associated with the ULX is located in the lower left (SE) of the plot. The cross represents the position of the ULX. The spatial resolution of this image is $1.94'' \times 1.20''$, $PA=8^\circ$, and the image has been made with ROBUST=1 weighting (slightly naturally weighted). The contour levels represent radio emission at -3, 3, 5, 7, 9, 10, 15, 20, 25, 50, 75, 100, 150, and 200 times the rms level of $20 \mu\text{Jy beam}^{-1}$.

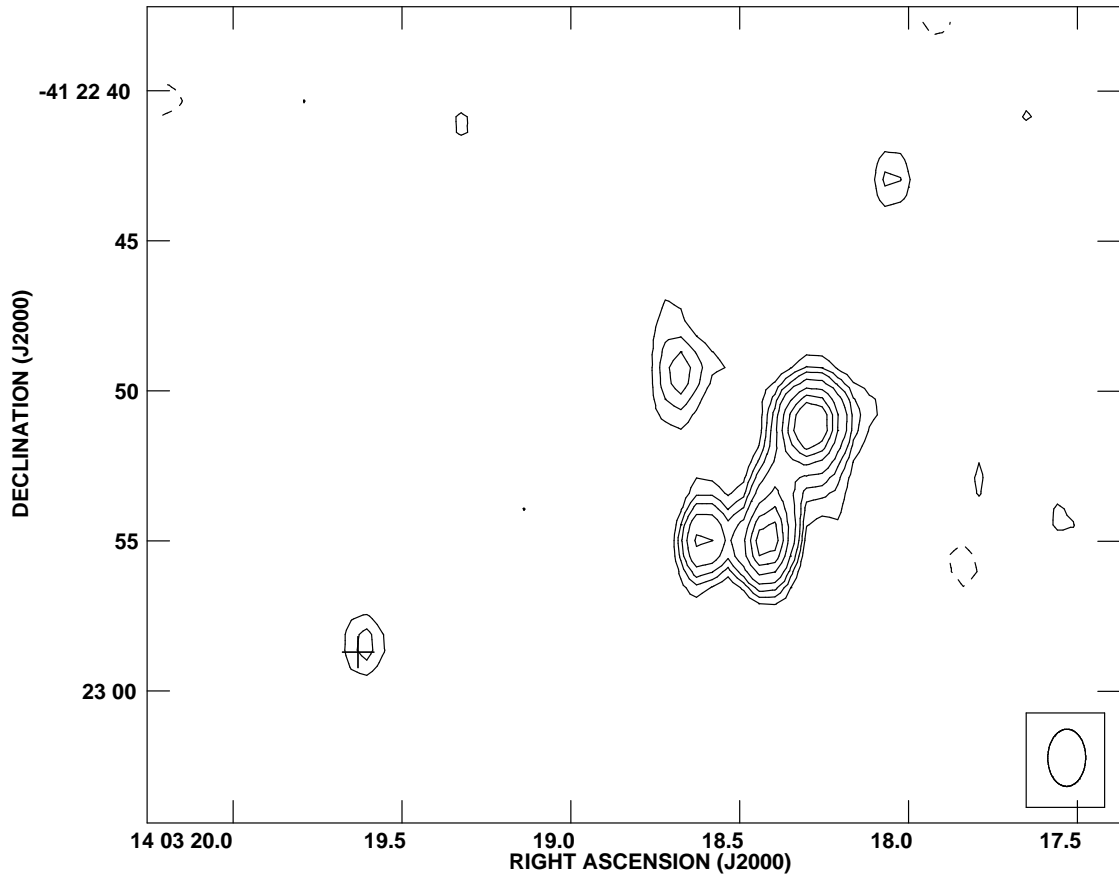


Fig. 2.— ATCA 4.8 GHz image of the radio emission in NGC 5408. The compact radio source associated with the ULX is located in the lower left (SE) of the plot. The crosses represents the position of the ULX. The spatial resolution of this image is $1.90'' \times 1.26''$, $PA=-55^\circ$, and contours represent radio emission at $-3, 3, 4, 5, 7, 9, 11, 13, 18, 21, 25, 30, 52, 84,$ and 136 the rms level of $32 \mu\text{Jy beam}^{-1}$. The image was made with uniform weighting (ROBUST=-5).

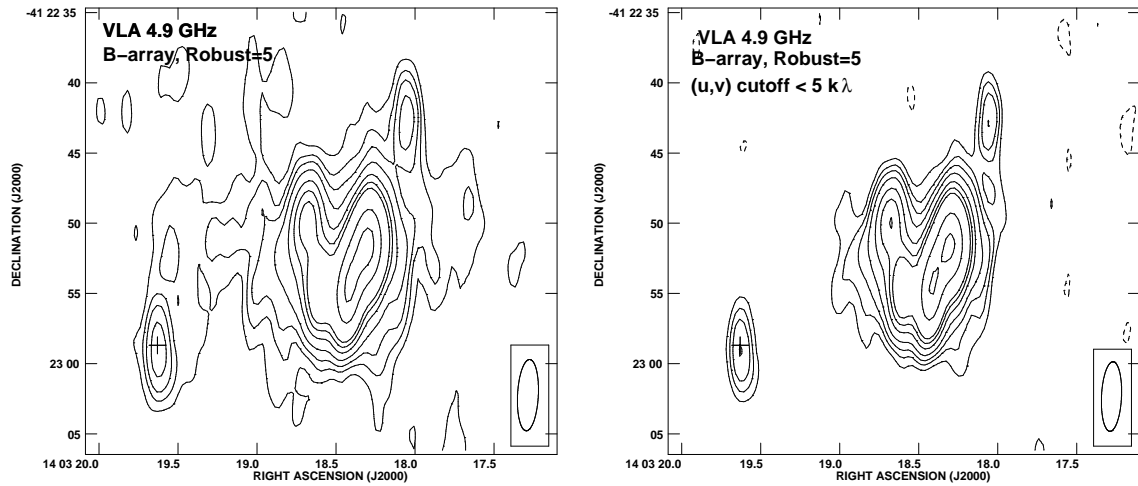


Fig. 3.— VLA 4.9 GHz B-array images of the radio emission in NGC 5408 made with ROBUST=5 (natural weighting). The left panel shows an image with a spatial resolution and the right panel shows an image made with data which have had a (u,v) cutoff $< 5 \text{ k}\lambda$ applied to them. In both cases, the spatial resolution is $5.0'' \times 1.5''$, $\text{PA} = -3^\circ$, and contour levels represent $-3, 3, 5, 7, 10, 15, 20, 25, 50, 75, 100, 125$ and 150 times the rms level of $20 \mu\text{Jy beam}^{-1}$.

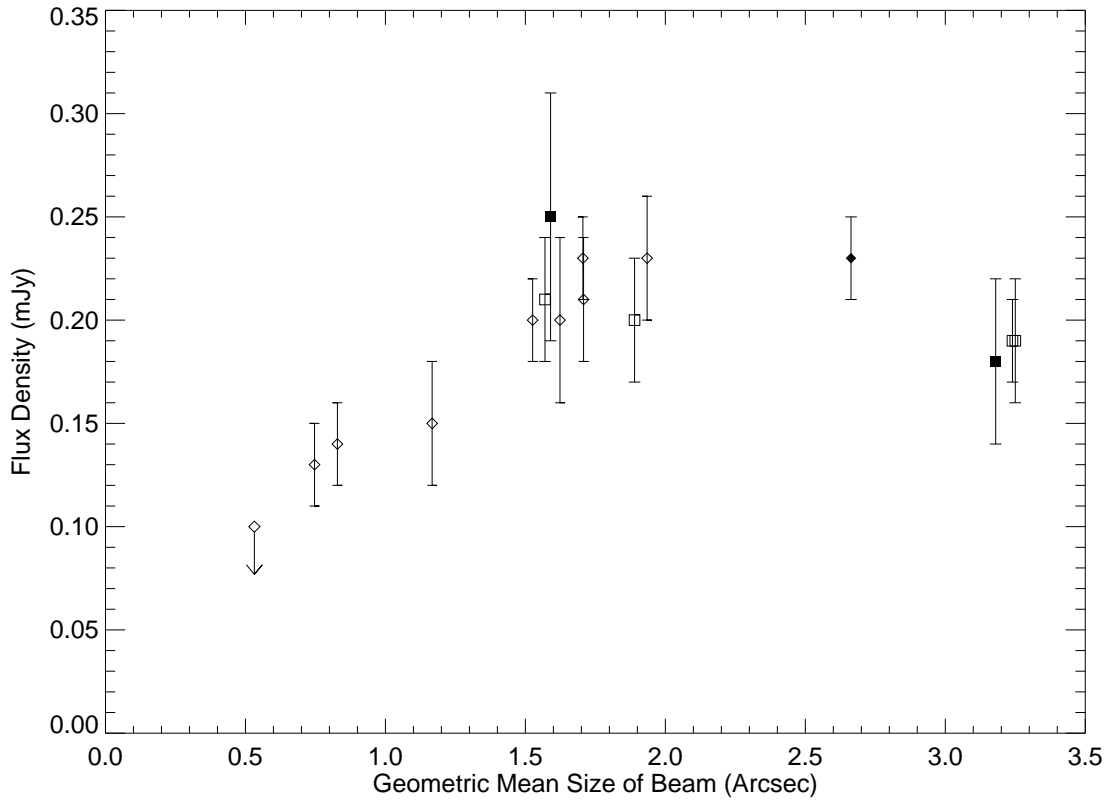


Fig. 4.— Flux Density vs. Geometric Beamsize for ATCA (squares) and VLA (diamond) radio observations at 4.9 GHz from this paper and from archival observations of Soria et al. (2006). Filled symbols represent measurements from images where the shortest (u,v) baselines have been removed to reduce contamination from the background galaxy. Error bars represent the error in fitting 2-D Gaussians to the unresolved point source.

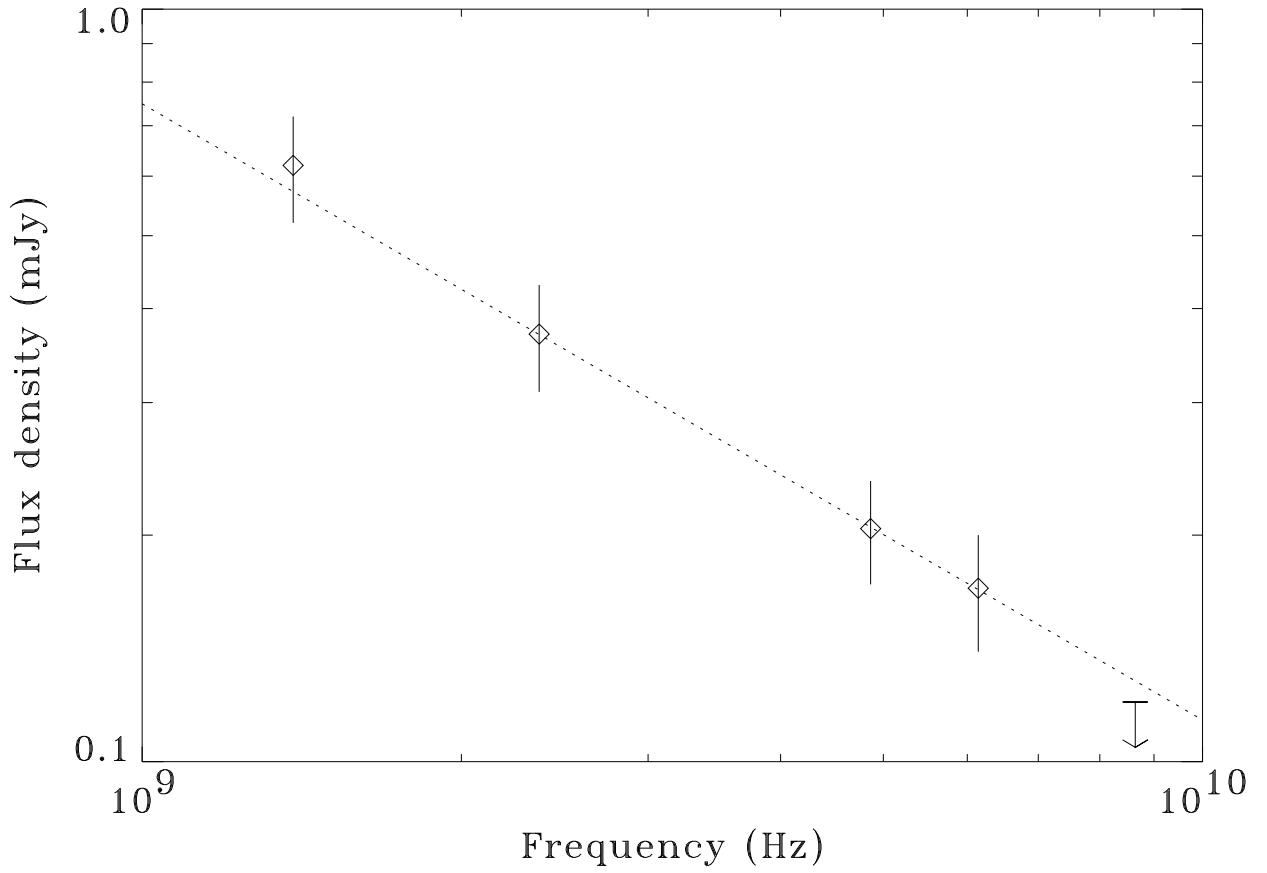


Fig. 5.— Flux density vs. frequency for the radio emission associated with NGC 5408 X-1. These measurements are from ATCA data, and the spectral index of $\alpha = -0.82 \pm 0.24$ is based on the 2.3, 4.9 and 6.1 GHz points. The 1.4 GHz flux density and 8.5 GHz upper limit are also included on this plot.

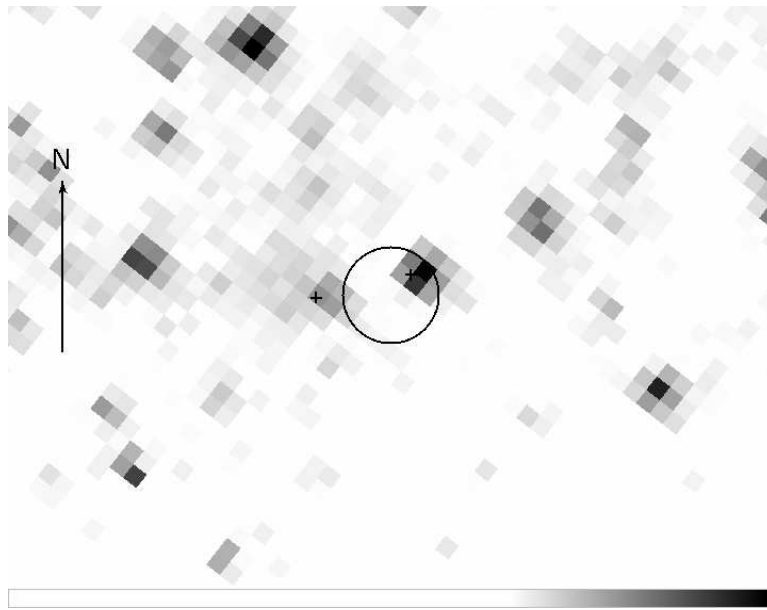


Fig. 6.— Image of the field near NGC5408 X-1 in the F606W band. The circle is centered at the position of the VLA counterpart of the ULX and has a radius of $0.28''$, which represents the relative position uncertainty including both the radio position uncertain and the optical astrometry uncertainty. Only one source lies within the error circle and we identify it as the likely optical counterpart of the ULX. The arrow has a length of $1''$ and points north.